The Meteoritical Society

Meteoritics & Planetary Science 42, Nr 12, 2079–2098 (2007)
Abstract available online at http://meteoritics.org

A hydrocode equation of state for SiO_2

H. J. MELOSH

Lunar and Planetary Laboratory, The University of Arizona, Tucson, Arizona 85721, USA
E-mail: jmelosh@lpl.arizona.edu

(Received 18 November 2005; revision accepted 13 May 2007)

Abstract–The thermodynamic properties of SiO_2 are approximated over a range of pressures and temperatures important under the extreme conditions achieved in impacts at typical solar system velocities from 5 to about 70 km/s. The liquid/vapor phase curve and critical point of SiO_2 are computed using the equation of state (EOS) program ANEOS. To achieve this goal, two shortcomings of ANEOS are corrected. ANEOS, originally developed at Sandia National Laboratories to describe metals, treats the vapor phase as a monatomic mixture of atoms, rather than molecular clusters. It also assumes a Morse potential for the expanded solid state. Neither of these assumptions is accurate for geologic materials, such as SiO_2, that contain molecular clusters in the vapor phase and are better described by a Mie-type potential in the solid state. Using the updates described here, an EOS adequate for numerical hydrocode computations is constructed that agrees well with shock data at pressures up to at least 600 GPa and temperatures up to 50,000 K. This EOS also gives a good representation of the liquid/vapor transition at much lower pressures and temperatures. The estimated critical point parameters for SiO_2 are P_c = 0.19 GPa, T_c = 5400K, ρ_c = 550 kg/m^3.

INTRODUCTION

Impact cratering is now recognized as one of the fundamental processes that shape solid bodies in our solar system. In the past half century, a large amount of information has been collected about impact events on the Moon, the planets, and on Earth. Two of the most remarkable events in Earth history, the origin of the Moon, and the extinctions at the end of the Cretaceous era, are now attributed to large impacts.

Numerical simulation of impacts by means of large computer codes has become one of the major tools for studying impact processes (experimental and field studies, of course, remain vital sources of information). Although recent progress in both computer hardware and the codes themselves has greatly expanded this field, progress has lagged in the accurate thermodynamic description of geologic materials at the extreme pressures and temperatures encountered in impacts. Part of this lag is due to the lack of good equation of state (EOS) models tailored to geologic materials, rather than metals. This paper is an attempt to narrow this gap by focusing on one particularly well-studied geologic material, SiO_2, and one EOS model, ANEOS.

The thermodynamic properties of geological materials are most efficiently represented on a pressure-temperature (*P-T*) diagram, because these variables readily summarize both the type of experimental conditions commonly used to study minerals, and because they can readily be correlated with conditions in the Earth's interior. Figure 1a shows the *P-T* phase diagram of SiO_2 as it is currently known (Presnall 1995), up to pressures of about 15 GPa and temperatures of 3500 K. Figure 1b is the same data, but plotted in a form that may be unfamiliar to earth scientists, as I have used a logarithmic axis for pressure and raised the upper limit of temperature to 7000 K. I have done this to capture the probable position of the liquid-vapor phase transition and the critical point where liquid and vapor merge indistinguishably into one another. The computation of this curve is the main subject of this paper, but a preview of the major results to illustrate their relation to older work may be useful.

The upper limits of experimental investigation of earth materials at pressures of tens of GPa and temperatures of a few thousand K may seem extreme enough, but they are actually very small compared to the pressures and temperatures achieved in impacts at solar-system velocities. At 20 km/s, which is typical of Earth-impact velocities, impacts of silicate asteroids onto silicate target rocks typically achieve pressures of hundreds of GPa and temperatures of tens of thousands of degrees. These extreme conditions are maintained only briefly, approximately for the length of time required for a shock wave to traverse the impactor, and so range from about 0.1 s for an impactor 1 km in diameter to

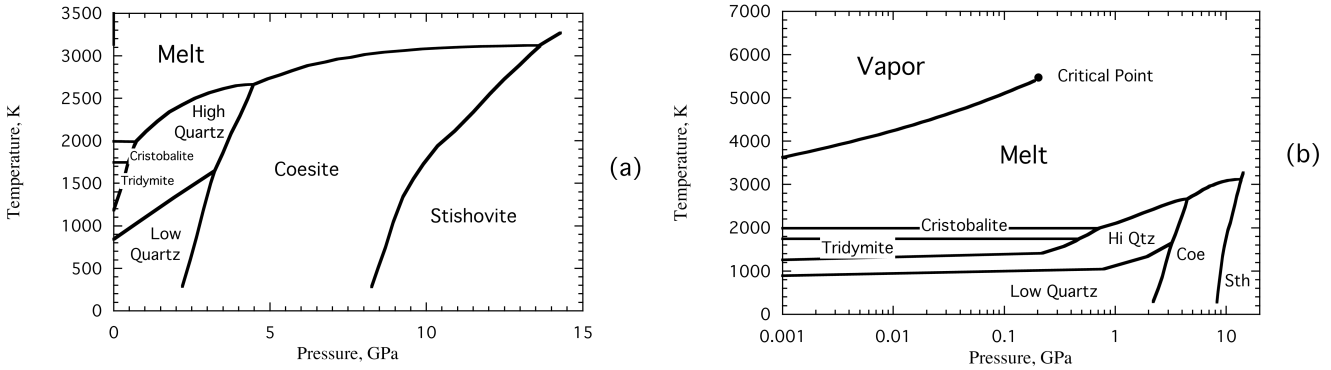

Fig. 1. The phase diagram of SiO_2 as currently known (data from Presnall 1995). The left diagram is plotted in conventional form with linear pressure and temperature axes. The right contains the same data, but uses a logarithmic pressure axis that expands the low-pressure region and permits the liquid/vapor phase curve and critical point to be shown on the same plot (but with a higher temperature limit). The ANEOS computation from which this phase curve is derived is described later in this paper.

seconds for dinosaur-killer asteroids 15 km in diameter. In laboratory experiments, these conditions are maintained for even briefer intervals, measured in microseconds or less, which presents one of the challenges in relating experimental studies to natural impacts.

Shock compression is a highly irreversible thermodynamic process (Melosh 1989). The narrow shock front that traverses both projectile and target conserves mass, energy and momentum, but it does not conserve entropy. Processes such as crushing, unreversed phase transformations, friction, thermal conduction, and radiation all act to deposit heat irreversibly in the compressed material. The results of shock compression experiments are frequently summarized by the Hugoniot curve, which is the locus of the final states achieved after a shock wave has compressed the initial material. Whether plotted as a function of pressure and volume or the equivalent (through the Hugoniot equations) particle velocity and shock velocity, the Hugoniot curve does not represent a thermodynamic path, but simply the ensemble of final states of a suite of shock compression events.

Once the shock compression event ends, rarefaction waves from surrounding regions of low pressure propagate into the compressed region and lower its pressure to ambient conditions. This decompression is generally adiabatic and, to a good approximation, isentropic. The series of pressures and temperatures passed through on decompression can be represented as a thermodynamic path on the traditional *P-V* or *P-T* diagrams. As Fig. 2 illustrates, however, this path can be very complex for a real substance such as SiO_2, in which the high-pressure coesite-stishovite phase transition or the liquid-vapor transition can greatly complicate the release curve. For this reason, a much better representation is a plot using the unfamiliar coordinates of pressure and entropy on a *P-S* diagram. To my knowledge, the first people to use such plots were Kieffer and Delany (1979), in the context of volcanic venting, a process that also approximates the isentropic expansion of a complex mixture of substances. Once the

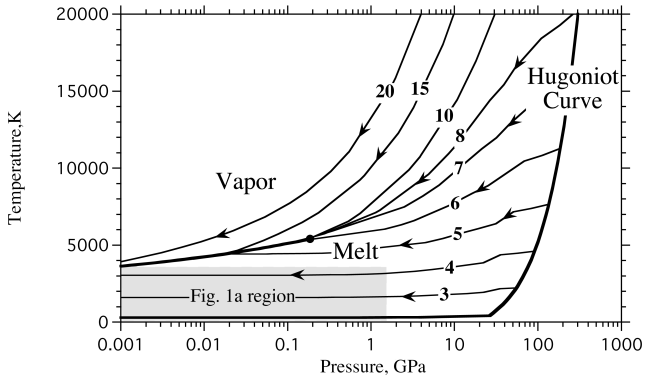

Fig. 2. Thermodynamic paths of the adiabatic release of shocked SiO_2 from high pressure on a log *P* versus *T* diagram. The Hugoniot curve, indicating the final result of increasingly strong shock compression of quartz, is shown as a heavy line, while the thin solid lines are decompression isentropes. The phase curve separating liquid and solid phases is shown as a heavy line and the critical point by a heavy dot. The numbers labeling the release adiabats are the particle velocities in the shocked material in km/s. These velocities can be interpreted as the outcome of an impact experiment between identical materials at twice the particle velocity. Thus, the curve labeled 7 is the release isentrope of a face-on impact between two quartz plates at 14 km/s. This isentrope approximately separates states that decompress first to a liquid that boils when it reaches the phase curve, from those so strongly shocked that they decompress as a vapor that then condense when the isentrope reaches the phase curve. The gray rectangle encompasses the entire pressure and temperature range in Fig. 1a.

Hugoniot curve is drawn on a *P-S* diagram, along with the phase boundaries of the substance it represents, the release isentropes are simply vertical lines, and the course of expansion subsequent to shock compression is easily followed. Figure 7 illustrates this type of diagram for SiO_2.

Knowledge of the thermodynamic cycle describing shock compression and release is important for a number of reasons. Understanding the aftermath of an impact, which includes an inventory of how much material was vaporized,

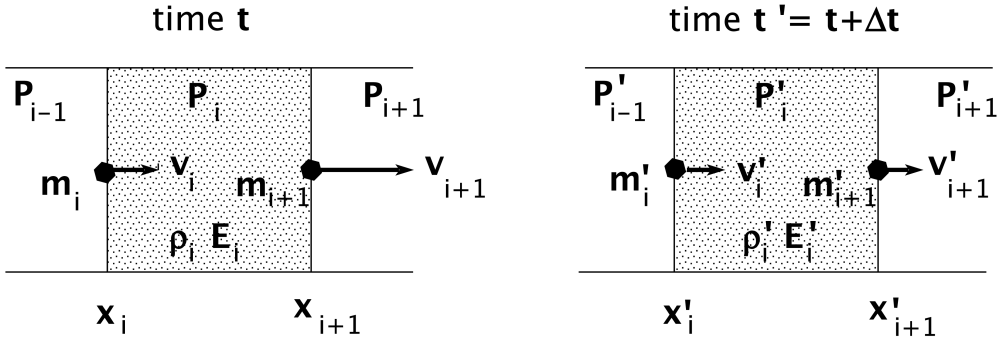

Fig. 3. Schematic illustration of a one-dimensional Lagrangian hydrocode computation. A single cell of this computation at an initial time t is shaded on the left half of the figure. The cell is bounded by two vertices shown as heavy dots. Position x, velocity v, and mass m are defined at each vertex. Cell-centered quantities are pressure P, internal energy E, and density ρ. The code advances from time t to $t + \Delta t$ by using Newton's laws of motion to compute the acceleration of the vertices and hence the new velocity, cell volume $x'_{i+1} - x'_i$, density, and internal energy, after which the solution cycle begins again, each time using the EOS $P'(\rho', E')$ to relate the new pressure to density and internal energy.

melted, or just heated, is important to the environmental effects of past and future impacts on the Earth or other planets. Shocked-damaged minerals and quenched metastable high-pressure phases such as coesite and stishovite are often used as diagnostic indicators of impact events, but their role in the impact process requires knowledge of how, when, and where they formed. The thermodynamic properties of any substance, such as SiO_2, are summarized by its EOS. The goal of this paper is to determine a reasonably accurate equation of state of SiO_2 that is valid over the entire range of conditions that are likely to be important in an impact event. The major reason for constructing this relationship is because it plays a vital role in numerical modeling of impact events.

WHAT IS AN EQUATION OF STATE AND WHY IS IT IMPORTANT?

A thermodynamic EOS is a functional relation that links the thermodynamic variables describing a substance. Most thermodynamics texts present the EOS as a relation linking the pressure P, temperature T, and density ρ (or its inverse, specific volume $V = 1/\rho$) in the form $P(\rho, T)$. Each substance and each state of a substance has its own unique EOS. Real materials are so complex that it is not, in general, possible to predict their equations of state from first principles: they must be determined empirically, by measurement. Nevertheless, a great deal of effort has been expended on approximating the EOSs of real substances and in using semi-empirical fits to extrapolate the measured data (e.g., Anderson 1995). EOS studies form a large portion of the effort of many physicists, geophysicists, and petrologists. However, most physicists are interested in ideal, or especially "clean" materials (specifically, not silicates or ices), and geophysicists and petrologists are mostly interested in solids, or, at most, partially molten materials. Only recently have high-speed impacts brought the importance of the solid/liquid/vapor transitions of silicates into prominence.

The most pressing need for better EOSs for geologic materials comes from the use of computer codes called "hydrocodes" (the name is mainly historical, referring to the fact that the first such codes treated materials as strengthless fluids. Modern "hydro"codes incorporate a variety of sophisticated material strength models and the name is no longer an apt description). These codes, which have been constructed over many years, are currently used to model the effects of impacts and explosions both at the laboratory scale and at scales much larger than possible in laboratory simulations (e.g., the Moon-forming impact). The use of such codes permits prediction of the changes in temperature, pressure, and velocity of materials involved in an impact.

The numerical simulation of impact processes rests on two fundamental pillars. One pillar is Newton's laws of motion (no solar-system impact process requires consideration of relativistic velocities!). Hydrocodes implement these equations in various ways, depending on whether the code is Eulerian, Lagrangian, or one of the newer smooth particle hydrodynamics (SPH) versions, but this has become a well-understood part of impact simulations (Anderson 1987).

The other basic pillar is the EOS, relating the pressure P to density ρ and internal energy E of each computational cell or region, or $P(E, \rho)$. This differs from the usual textbook relation $P(\rho, T)$ because the mechanical part of the code computation most readily determines E, not T. Although this structure is a bit non-standard, there is a close connection between the two representations and it is usually possible to translate from one to another, depending on the particular computational method used.

Figure 3 illustrates the essentials of a hydrocode computation. For simplicity I have chosen a one-dimensional model (most modern codes work in three dimensions) and for definiteness I have illustrated a Lagrangian type of computation, in which material remains in the same cell throughout the computation. The region to be simulated is

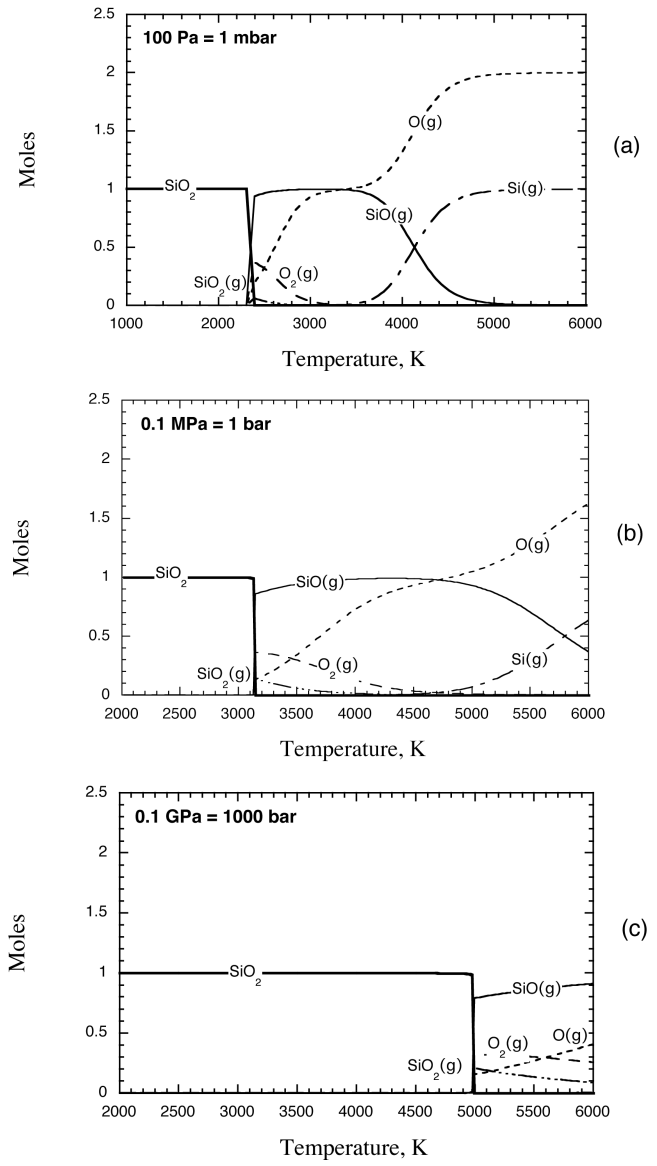

Fig. 4. Species present in the vapor phase of SiO_2 as a function of temperature for three pressures. a) P = 100 Pa. b) P = 0.1 MPa (one bar). c) P = 0.1 GPa. Note that the vapor phase is predominantly SiO plus O_2 just above the vaporization temperature, with an admixture of about 20 mole% of SiO_2. At higher temperatures, these molecular clusters break down into atoms so that the high-temperature limit is a mixture of monatomic Si and O gases. Computed from the HSC Chemistry program 5.0 (Roine 2002), assuming ideal gases in the vapor phase.

divided into a large number of "cells," which are separated by "vertices." Quantities in the computation are either cell-centered, such as pressure, energy, and density, or vertex-centered, such as position and velocity. Mass is typically associated with both cells and vertices. In this example, the vertex mass would equal the sum of half the mass located in each cell adjacent to the vertex. The Newtonian dynamical relation *force* = *mass* × *acceleration* is then be applied to each vertex. At the beginning of a time cycle the velocity and position of each vertex is known, as is the energy and density in each cell. The pressure in the cell is then computed from the EOS $P(\rho, E)$. The force on each vertex is then the sum of the pressures in each adjacent cell times the area of the interface. New velocities and positions are computed from *acceleration* = *force/mass*, the change in density of the cell is computed from its initial mass and change of volume, and a new internal energy is computed from the relation *work* = *force* × *distance*. The cycle is then repeated until the final result is achieved. Most impacts occur so quickly that thermal conduction is not important, and the temperatures reached in solar system impacts are not high enough to consider heat transfer by thermal radiation.

The central role of the EOS is evident from this description. The problem is that very few accurate EOSs exist for geological materials, and at present this is one of the main factors limiting our ability to numerically model solar system impacts. In Appendix II of *Impact cratering: A geologic process* (Melosh 1989), I summarized the EOSs in common use, along with their virtues and limitations. Most of the past effort on EOSs at high pressures and temperatures has focused on metals, because engineered structures are mostly made from metals. In this paper, I focus on a well-defined geologic material, SiO_2, not because large parts of the Earth and planets are made mainly of it, but because there is more detailed thermodynamic data on SiO_2 than on nearly any other geologic material. My philosophy is that if I can achieve an adequate description of SiO_2 over the whole range of interest for impacts, then the methods used for this specific material may be applied more generally to other, more widely distributed, geologic materials such as basalt or water ice (ANEOS parameter sets already exist for these materials, as well as for forsterite, but the older versions of ANEOS have drawbacks that are alleviated in the work described below). The basic foundation for this EOS is the computer code ANEOS. I begin with a discussion of the properties of SiO_2 at high pressures and temperatures. This will provide a foundation for understanding the modifications that must be incorporated into ANEOS. I then present a detailed discussion of the structure of ANEOS, its virtues, and its drawbacks for the representation of geologic materials. This section will also describe cures for two of its major problems. I then show how the upgraded ANEOS provides a greatly improved representation of the SiO_2 EOS.

SiO_2 AT HIGH PRESSURES AND TEMPERATURES

The currently accepted phase diagram of SiO_2 is summarized in Fig. 1. Much of the detail of the various phases is too complex to be adequately described by a hydrocode EOS, nor is it needed for present modeling purposes. As shown in Fig. 5, only the large density change across the quartz-stishovite phase transformation shows up in the

Hugoniot plot. On the other hand, very little is known about the behavior of SiO_2 over the very large temperature and pressure range that includes vaporization, the critical point, and high-pressure supercritical fluid regimes.

The best previous work on SiO_2 in these regimes is the paper by Ahrens and O'Keefe (1972). Basing their work on the then-available thermodynamic data, they proposed that the vapor phase of SiO_2 is mainly composed of the diatomic molecules SiO and O_2. Figure 4 shows the result of a modern equilibrium thermodynamic computation of the species in the gas phase over liquid SiO_2 for three pressures, using the commercial HSC 5.0 chemistry package (Roine 2002). The gas phase is treated as ideal, so the computation is not valid near the critical point. Although the dominant species are indeed SiO and O_2, there is about 20 mole% additional SiO_2 gas in the mixture. This admixture alters the slope of the liquid/vapor phase curve in Fig. 8 below and yields an apparent enthalpy of vaporization of 481 kJ/mole derived from the phase curve of Hidalgo (1960), 484 kJ/mole from the detailed analysis of Schick (1960) and 425 kJ/mole from a fit to the low-pressure data of Mysen and Kushiro (1988), rather than the 536 kJ/mole used by Ahrens and O'Keefe (1972).

The SiO_2 phase curves of Schick (1960) and Hidalgo (1960) deserve some comment here. The phase curve published by Hidalgo appears only as an appendix of his paper, which offers no information about how it was obtained. The paper of Schick is a very careful and detailed thermodynamic analysis of the phase curve from a combination of theory and experimental studies. Both papers appeared in the same year and both men worked at Avco Corporation at the time, so there may have been some connection between these studies. Schick explicitly included the multispecies equilibrium in the gas phase, while Hidalgo's phase curve is numerically similar, but not identical, to the SiO pressure versus temperature relation of Schick. Insofar as Hidalgo did not describe the origin of his curve, the analysis of Schick is preferred here.

There is a long history of attempts to measure or compute the liquid-vapor phase curve of both pure SiO_2 and SiO_2-rich compositions at atmospheric pressure and below. The vapor pressure over silicate melts of tektite compositions was measured by Walter and Carron (1964) and Centolanzi and Chapman (1966). Schaefer and Fegley (2004) performed thermodynamic computations of silicate evaporation at low pressure, using thermodynamic data from a number of Russian investigations (Shornikov et al. 1998a, 1998b, 1998c).

Figure 4 shows that at sufficiently high temperatures (near 6000 K at 1 bar pressure) the gas phase becomes predominantly monatomic, but there is a broad range of temperature above the vaporization temperature at about 3200 K where the gas is a complex mixture of mainly diatomic species. Figure 9 illustrates another aspect of the HSC computation, in which the entropy of the gas phase at 1 bar is compared to the ANEOS computation described below. The entropy also rises rather steeply above the vaporization temperature, reflecting the dissociation of the diatomic clusters into a monatomic gas mixture.

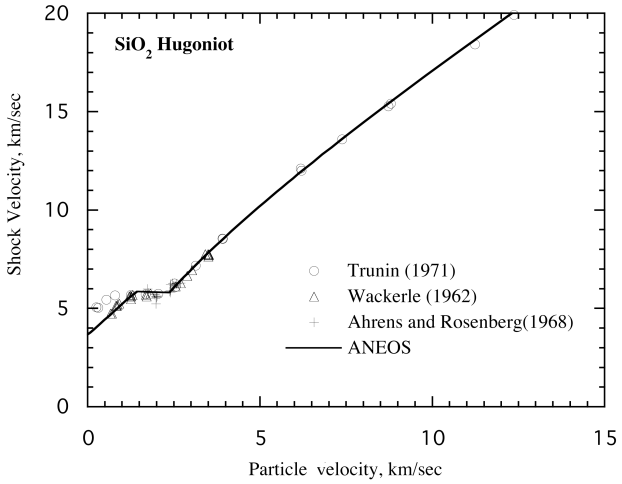

Fig. 5. Comparison between the Hugoniot curve computed for SiO_2 by the ANEOS equation of state described in this paper and data from Trunin et al. (1971), Wackerle (1962), and Ahrens and Rosenberg (1968). The Hugoniot is shown in the convenient coordinates of shock velocity versus particle velocity, which are equivalent to the more conventional coordinates pressure, specific volume through the Hugoniot equations (Melosh 1989). The computed curve agrees well with data above a particle velocity of 1 km/s (about 15 GPa), but at low velocities it disagrees with the Trunin et al. data. This discrepancy may be explained by the fact that the Trunin et al. experiments used polycrystalline quartz, while the others used single crystals, although reaction kinetics may also be playing a role (see text for further discussion).

THE CRITICAL POINT OF SiO_2

An important aspect of the EOS of any fluid is the location of its critical point. At pressures above the critical pressure, liquid and vapor states merge together. Separate liquid and vapor phases can only exist at pressures below the critical point. In a typical hypervelocity impact, the initial shock pressures and temperatures greatly exceed the critical point of any known substance. The adiabatic pressure release following shock compression initially proceeds through a supercritical fluid, and only as the pressure drops below the critical point can separate liquid and vapor phases come into existence. Because the gas phase can drive vigorous expansion of the liquid/vapor mixture, it is important to know when a vapor phase appears and how much of it forms at a given pressure and temperature. Furthermore, any partition of chemical species between the gas and liquid phase can take place only when both are present, so the critical pressure P_c and temperature T_c are of great significance for the outcome of high-speed impact processes.

The critical point of SiO_2 has never been measured experimentally. Several estimates of its location have

Table 1. Critical point parameter estimates for SiO_2.

Method	Pressure (GPa)	Temperature (K)	Density (kg/m^3)	Molecular weight (gm/mole)	Critical ratio
Ahrens and O'Keefe (1972)	0.642	13,500	637	40	0.36
				60	0.54
New Young and Adler (1971)	0.60	12,400	650	40	0.36
				60	0.54
Pauling (1988), SiO + ½ O_2	0.652	14,050	595	40	0.37
Pauling (1988) SiO_2	0.322	12,990	595	60	0.30
Guldberg's rule	0.243	4690	839	40	0.30[a]
(Hirschfelder et al. 1964)	0.162	4690	839	60	0.30[a]
Bobrovskii et al. (1974)	0.54	5400	741	40	0.65
				60	0.97
Vapor curve extrapolation, this work	0.219	5397	650[a]	40	0.30[a]
	0.140	5181	650[a]	60	0.30[a]
ANEOS, Morse potential	0.0239	5071	72.6	40	0.30
				60	0.47
ANEOS, Mie potential, no critical point adjustment	0.444	6214	690	40	0.50
				60	0.75
ANEOS, Mie potential, including critical point adjustment	**0.189**	**5398**	**549**	**40**	**0.31**
				60	**0.47**

[a]Assumed value.

appeared in the literature and, if they are correct, indicate that the pressure and temperature of the critical point are beyond our present ability to study experimentally. However, for a successful EOS, a good approximation to its location is necessary.

Ahrens and O'Keefe (Ahrens and O'Keefe 1972) used a hard-sphere model originally derived for metals (Young and Alder 1971) to estimate a critical pressure of 0.642 GPa and a temperature of 13,500 K (see Table 1). They assumed that the dominant vapor species are the diatomic molecules SiO and O_2, from which they derived an enthalpy of vaporization of 803.7 kJ/mole of SiO + 1/2O_2 from the thermodynamic data then available. A recalculation using the same method, but with data from the current NIST/JANAF tables (Chase 1998), gives a similar result for pressure, but a temperature about 1000 K lower (Table 1).

Several empirical methods exist for estimating the critical point. Most of these are based on the "law of corresponding states," that asserts that the thermodynamic properties of all substances are the same when expressed in "reduced" units of pressure divided by the critical pressure P/P_c and temperature divided by the critical temperature, T/T_c. Furthermore, the law implies that product of critical parameters, $P_c/R\rho_c T_c$, is a universal constant called the "critical ratio," which is approximately equal to 0.3 (Hirschfelder et al. 1964). The Van der Waals equation predicts that this ratio is 3/8 = 0.375, which is higher than observed for most substances. Unfortunately, this relationship is somewhat ambiguous because one must specify the molecular weight of the substance to evaluate it. Ahrens and O'Keefe assume that both the liquid and vapor state near the critical point are composed of SiO plus O_2 clusters, so that the mean molecular weight is 40 gm/mole. However, most tabulations of this ratio use the formula weight of the substance and do not attempt to guess what form the molecular clusters take. Table 1 thus evaluates the critical ratio at both molecular weights.

"Guldberg's rule" (Hirschfelder et al. 1964, p. 234ff) states that the critical temperature of a substance is approximately 3/2 of the vaporization temperature at 1 bar, which yields a T_c about 4690 K for SiO_2 (using a vaporization temperature of approximately 3127 K), very different from the hard-sphere model of Ahrens and O'Keefe. A method due to Pauling (1988, p. 338) is based on the heat of vaporization and yields a critical point close that of Ahrens and O'Keefe (see Table 1). Both Guldberg's rule and Pauling's method implicitly assume that either the boiling point or melting point at 1 bar occur at the same value of the reduced pressure and temperature for all substances—i.e., that the critical point of all materials is nearly the same. Clearly, such rules of thumb may be badly violated when applied to a material, such as SiO_2, whose critical point differs so greatly from more familiar vapors.

In the process of constructing an ANEOS equation of state for SiO_2, I found it impossible to achieve the Ahrens and O'Keefe estimate of the critical point and at the same time match the observed liquid/vapor saturation curve. The problem is that, on an Arrhenius-type plot of log P versus 1/T, Ahrens and O'Keefe's critical point does not lie on the extrapolation of the liquid/vapor saturation curve. However, the critical point must lie on this curve. For most materials the saturation curve is nearly a straight line on an Arrhenius plot. I thus tried a new approach in which I used the empirically validated liquid/vapor saturation curve of Schick (1960), linearly extrapolated the relation between P and T on an Arrhenius plot, assumed that the critical ratio is exactly equal

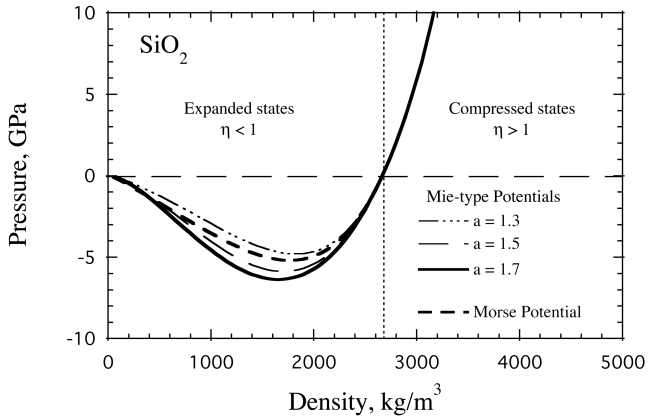

Fig. 6. The cold compression portion of the EOS, emphasizing the expanded region with density less than the cold reference density ρ_{00}. The plot shows three values of the Mie exponent a and the Morse potential. Note that the energy integral, Equation 3, of all these curves is the same, in spite of appearances. The $1/\eta^2$ term in Equation 3 puts a strong emphasis on the behavior of the cold pressure near $\eta = 0$, which is different for each curve.

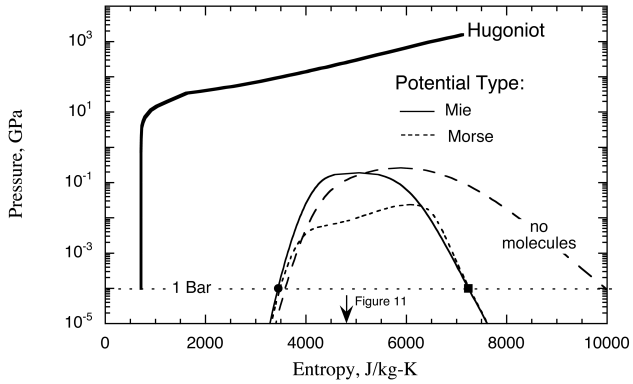

Fig. 7. Pressure-entropy representation of the ANEOS equation of state. The heavy solid line is the Hugoniot curve. The thin solid line is derived from the ANEOS parameters for the Mie cold potential in Table 3. The computation shown by the short dashed line uses the same input parameters, but employs the Morse potential illustrated in Fig. 6. Its behavior near the critical point is pathological, showing the incipient formation of a second peak. The long dashed line illustrates the result of omitting molecular clusters (in this case, the Mie exponent $a = 1.5$ and E_{vap} was increased to 2.08×10^7 J/kg to give the correct vaporization temperature). The vapor phase entropy is much too high because in this case the vapor phase is a monatomic gas of Si and O atoms. The filled circle and square are the entropies of the liquid and vapor phases, respectively, from the HSC computation listed in Table 2. The long vertical arrow at entropy 4789 J/kg-K indicates the release path from shock compression at a particle velocity of 7 km/s, and indicates the thermodynamic path traversed by the expanding gas cloud shown in Fig. 11.

to 0.3, and accepted a critical density of 650 kg/m^3, close to the estimates of all methods of evaluating the critical point parameters. The result, listed in Table 1, agrees reasonably well with that computed from ANEOS.

This method does not make any implicit assumptions about the position of the critical point and guarantees that the critical point lies on the extrapolation of the phase curve. It thus seems superior to the previous rules of thumb used to estimate the critical parameters, as well as to the Young and Adler (1971) hard-sphere model that was, after all, constructed for metals, not oxides, and seems to fail badly for SiO_2 (the authors also note that it fails badly for some metals as well).

Note that the initial results from ANEOS did not yield a critical ratio near 0.3, even for an assumed molecular weight of 40. However, an adjustment of the shape of the cold-compression curve, described below, succeeded in adjusting the critical parameters such to yield a critical ratio nearly equal to 0.3. Although the Morse potential computation reported there does give a critical ratio near 0.3 without any adjustments, the vapor curve on the *P-S* plot in Fig. 7 is clearly pathological, having a shape that approaches a double-peaked curve, which would give an unrealistic multiple critical point.

THE ANEOS EQUATION OF STATE

The ANEOS equation of state was developed at Sandia National Laboratories, principally by Sam Thomson, between about 1970 and 1990 (Thompson 1973, 1990; Thompson and Lauson 1972a, 1972b). The name ANEOS emphasizes that it is based on a series of ANalytic approximations to various terms in the EOS. ANEOS grew out of what was originally a tabular EOS that had analytic extensions to regions of density and temperature not covered by the tables (Thompson and Lauson 1972a). In later work (Thompson and Lauson 1972b), Thompson evidently decided that the difficulties of locating phase boundaries in a purely tabular EOS were so severe that an approach using analytic functions throughout offered many advantages in constructing a thermodynamically consistent EOS.

The basic approach in ANEOS is to start with an analytic expression for the Helmholtz free energy, $F(\rho, T)$. Because each hydrocode time cycle begins with freshly computed values of density ρ and internal energy E, this is not precisely the form most useful for hydrocode computations. However, a simple Newtonian iteration of the temperature T to find a target value of the internal energy E is typically very quick and reliable because the computation itself determines the slope dE/dT (equal to the heat capacity C_V) at constant density. The heat capacity is invariably positive and non-zero, so the iteration almost never fails. As a bonus, this method also returns the temperature, which is not readily accessible from many widely used hydrocode EOS, such as the Tillotson equation (Tillotson 1962) or a Mie-Gruneisen EOS (Zharkov and Kalinin 1971).

The Helmholtz free energy F is the most natural thermodynamic potential to use in impact computations because temperature T and density ρ are its "fundamental

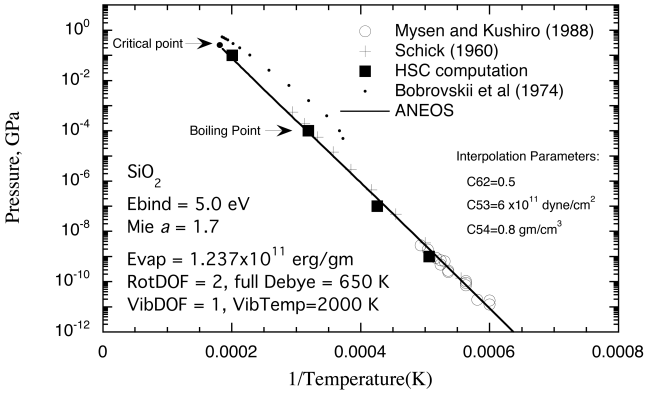

Fig. 8. Summary plot of the saturated vapor curve of SiO_2 on an Arrhenius plot of pressure versus $1/T$. The legend on the plot summarizes the ANEOS input parameters for the computation of the heavy line. The circles are low-pressure data from Mysen and Kushiro (1988), the crosses are derived from the vapor phase curve of Schick (1960), and the squares are chemical equilibrium computations from HSC 5.0. The small dots are from a computation by Bobrovskii et al. (1974), which are based on a model similar to the present modified version of ANEOS but fit to older, somewhat different thermodynamic data on SiO_2.

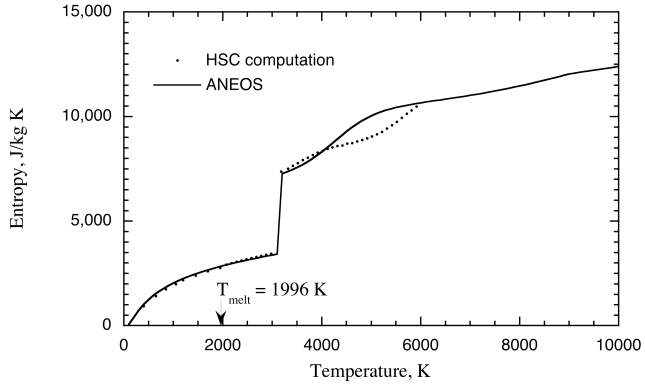

Fig. 9. Entropy of SiO_2 as a function of temperature at 1 bar pressure. The small squares are the HSC 5.0 computation and the solid line is from ANEOS. Note only a small step in the HSC occurs at the high cristobalite melting point of 1996 K, while a large step occurs at the vaporization temperature. ANEOS and HSC do not match well between about 4500 and 6000 K because of the assumption that only one binding energy characterizes the decomposition into Si and O_2, whereas two are actually involved. Nevertheless, ANEOS gives a good average representation of the curve over most of its range.

variables," such that $dF = -SdT + P/\rho^2 d\rho$, where S is entropy and P is pressure (Denbigh 1971). It thus follows that the entropy and pressure of any material can be derived from F by the equations:

$$S = -\left.\frac{\partial F}{\partial T}\right|_{\rho} \qquad (1)$$

$$P = \rho^2 \left.\frac{\partial F}{\partial \rho}\right|_{T}$$

Other useful thermodynamic functions, such as the internal energy $E = F + TS$, Gibbs energy $G = E + P/\rho - TS$, heat capacity C_V, and the derivatives $dP/d\rho$ and dP/dT can easily be derived from these fundamental equations.

ANEOS separates the Helmholtz free energy into three parts, an approximation justified by the separability of the wave function into nuclear and electronic components (Zel'dovich and Raizer 1967; Zharkov and Kalinin 1971):

$$F(\rho, T) = F_{\text{cold}}(\rho) + F_{\text{thermal}}(\rho, T) + F_{\text{electronic}}(\rho, T) \qquad (2)$$

The first term, F_{cold}, contains the parts of the atomic interactions that do not depend on temperature, such as the interatomic potential. F_{thermal} contains the temperature-dependent parts of the interatomic forces. Thompson used the subscript "nuclear" for this term, but this terminology is misleading to an earth scientist—it does not refer to nuclear energies, which ANEOS does not evaluate, but to the thermal energy of collective motion of the nuclei and their associated electrons. The "thermal" term vanishes when $T = 0$ and approaches a perfect gas EOS at sufficiently high pressure and low density. $F_{\text{electronic}}$ contains energies related to ionization of atoms and is only important at very high temperatures and low densities.

Because pressure and entropy are linear functions of F (Equation 1), they can also be decomposed into a sum of three terms (two in the case of entropy, because F_{cold} depends only on density, not temperature). The original ANEOS equation of state was developed to describe metals, not geologic materials, and the choices of analytic approximations to the three terms in Equation 2 were made specifically for metals. However, geologic materials are often complex chemical compounds lacking metallic bonds, and these approximations may not work well for them. Experience in using and modifying ANEOS over the past several years has indicated a number of areas that need alteration for geologic materials.

The most serious defect of ANEOS is that it treats the gas phase as a mixture of perfect monatomic gases. The vapor phase of such a monatomic gas has very high energy and entropy compared to a more realistic gas containing molecular clusters. This means that very little vapor may be generated in a hydrocode computation that uses ANEOS because of the high energetic cost of producing it. Problems due to this lack of vapor production have been noted in a number of hydrocode computations, and directly inspired the alterations to ANEOS described in this paper (Melosh and Pierazzo 1997).

In addition to modifications of the "thermal" part of the Helmholtz free energy, there are also changes needed in the "cold" term. To date, no modifications to the "electronic" terms have been required. The following sections briefly outline the changes necessary to the basic ANEOS equation of state.

Table 2. Target and final thermodynamic properties of SiO_2.

Property	Source	Target	ANEOS result
T_{vap}, vaporization temperature at 1 bar, K	NIST/JANAF (Chase 1998)	3127	**3157**
	Schick (1960)	3070	
	Hidalgo (1960)	3141	
	Ahrens and O'Keefe (1972)	3175	
	Barin (1989)	3223	
S_{liq}, liquid entropy at 1 Bar, J/kg-K	HSC (Roine 2002) equilibrium chemistry computation	3447	**3443**
	NIST/JANAF (Chase 1998)	3507	
S_{vap}, vapor entropy at 1 Bar, J/kg-K	HSC equilibrium chemistry computation	7237	**7240**
	NIST/JANAF (Chase 1998)	7267	
P_{Δ}, triple point pressure, Pa	Pressure from Schick (1960) vapor curve at T_{melt} = 1996 K	3.2	**2.7**
	Least squares fit to Mysen and Kushiro (1988) at 1996 K	1.9	

"COLD" TERM IN THE HELMHOLTZ FREE ENERGY

The "cold" term of the ANEOS equation of state is important not only for densities larger than the reference density at zero temperature, ρ_{00}, but also for densities much lower than those considered normal. In such "expanded" states, where the density ratio $\eta = \rho/\rho_{00} < 1$, this term represents the energy of interaction of atoms located farther apart than their low-temperature and pressure-equilibrium positions.

The "compressed" region, $\eta > 1$, is well-treated by the original ANEOS and provides a good representation of the high-pressure EOS, as demonstrated by Fig. 5, which shows a good fit between the observed Hugoniot shock compression curve and the ANEOS prediction. The only caveat in this generally good fit is that ANEOS treats high-pressure phase transitions as a modification of the cold compression term alone. This means that the pressure of the phase transition depends only slightly on temperature, a result that disagrees with the obvious slope of the coesite-stishovite phase curve in Fig. 1. The fixed-pressure phase transformation also prevents the introduction of separate liquid and solid phases in ANEOS (the liquid/solid phase boundary is too difficult to locate), so the condensed liquid and solid states cannot be distinguished when a high-pressure phase transformation is introduced. Furthermore, as noted by Ivanov (2003), the lack of thermal differences between the high-pressure and low-pressure phases means that, among other things, the thermal expansion coefficient of the high-pressure phase is the same as the low-pressure phase. This unrealistic result sometimes leads to problems in defining the initial conditions in geological simulations where gravitational overburden pressures are significant. The treatment of high-pressure phase transitions is an area that obviously needs improvement in ANEOS. To be fair, the author of ANEOS, Sam Thomson, was unhappy with this treatment and stated that it was "provisional" until a better formulation was implemented (Thompson and Lauson 1972b). Unfortunately, Thompson died before this was completed.

The expanded region of the cold compression term, $\eta < 1$, plays a surprisingly important role in the liquid/vapor transition. The energy of separation, which we denote here as the vaporization energy, E_{vap}, is the total energy needed to separate the molecules composing the liquid or solid phase to great distances from one another at zero temperature (in the original ANEOS, in which molecules did not exist, this was the energy to separate the atoms from one another. In the present molecular implementation, this energy of vaporization does not include the molecular binding energy). The vaporization energy is thus:

$$E_{vap} = -\int_0^{\rho_{00}} \frac{P_c(\rho)}{\rho^2} d\rho \tag{3}$$

where ρ_{00} is the density of the solid at zero pressure and temperature. The cold contribution to the pressure $P_c(\rho)$ must clearly be negative (tensional) in this region if E_{vap} is to be a positive number. This energy, in conjunction with the heat capacity of the solid and vapor states, determines the vaporization temperature (boiling point at 1 bar) of the material. The cold pressure must, however, vanish at sufficiently low density if the material is to act like a gas at low density. $P_c(\rho)$ must thus vanish at $\rho = \rho_{00}$ and in the limit $\rho \rightarrow 0$, but is negative in between. There is thus a pressure minimum at some intermediate density smaller than ρ_{00}.

One of the most important roles of the pressure minimum in the expanded state is to create a trough in the surface of the Gibbs free energy. This is the "plait" in the energy surface that occupied much of Van der Waals career (Sengers 2002). No other term in the EOS creates such a minimum. The density of the liquid and vapor states are determined at a given temperature by the equality of both the total pressure and Gibbs energy on either side of this minimum, so its existence is the only feature of the thermodynamic surface that assures a separation between these two states. In addition, the position of the critical point is determined by the interaction between the minimum in the cold-pressure curve and the thermal contributions to the liquid and vapor phases, so that the cold-expanded pressure curve is of overriding importance in determining the liquid/vapor phase curve.

The original version of ANEOS incorporated a Morse potential to describe expanded states (Thompson and

Table 3. Input parameters for ANEOS SiO_2.

Input	Description	Source	Value
Nelem	Number of elements in SiO_2	Si and O	2
Type	Type of EOS	4 is a full solid/liquid/vapor treatment	4
Rho0	Density at reference condition	Alpha quartz (Weast 1972)	2.65 gm/cm^3
Temp0	Reference temperature	Standard temperature	0 (defaults to 273 K)
Press0	Reference pressure	Standard pressure	1 bar
Cbulk	Bulk sound speed in reference state	Marsh (1980)	3.68×10^5 cm/s
Grun	Gruneisen ratio in reference state	This work; see text	0.618
Tdebye	Debye temperature, average over quartz, cristobalite and liquid to 3100 K	Fit, this work. Data from HSC chemistry computation.	650 K (uses full Debye treatment)
S	Slope of particle-velocity, shock velocity curve for quartz	Marsh (1980)	2.12
3*C24	High pressure exponent	Extrapolates to Thomas-Fermi limit at ultra-high pressure	2
Evap	Energy of vaporization	Fit, this work	1.237×10^{11} erg/gm
Tmelt	Melting temperature (high cristobalite)	NIST/JANAF (Chase, 1998)	1996 K
C53	Critical point adjustment	This work	0.8
C54	Critical point adjustment	This work	6×10^{11} dyne/cm^2
H0	Thermal conduction	Not used	0
C41	Thermal conduction	Not used	0
Rhomin	Minimum density	This work	0 (defaults to 0.9 rho0)
D1	Density at onset of high pressure phase transition (hppt)	This work, based on data in Marsh (1980)	3.5 gm/cm^3
D2	Density at completion of hppt	This work, based on data in Marsh (1980)	4.3 gm/cm^3
D3	Pressure at center of hppt	This work, based on data in Marsh (1980)	2.1×10^{11} dyne/cm^2
D4	$dP/d\eta$ at end of hppt	This work, based on data in Marsh (1980)	1.8×10^{12} dyne/cm^2
D5	$d^2P/d\eta^2$ at end of hppt	This work, based on data in Marsh (1980)	6×10^{12} dyne/cm^2
Hfusion	Enthalpy of fusion	Not used	0
Rholiq	Liquid density	Not used	0
Up	Cold compression limit	Not used	0
L0	Cold compression limit	Not used	0
Alpha	Liquid Gibbs surface shape parameter α	Not used	0
Beta	Liquid Gibbs surface shape parameter β	Not used	0
Gamma	Liquid Gibbs surface shape parameter γ	Not used	0
C60	Interpolation parameter	Not used	0
C61	Interpolation parameter	Not used	0
C62	Liquid/vapor convergence parameter, C60 = $(1 - b)$	This work	0.5
IonFlag	Ionization model	0 = Saha, 1 = Thomas-Fermi tabular	0
Eshift	Reactive chemistry, energy shift	Not used	0
Sschift	Reactive chemistry, entropy shift	Not used	0
Atoms[a]	Number of atoms in molecular clusters, $n + m$	This work	2
Ebind[a]	Molecular cluster binding energy, E_B	Fit, this work	5 eV
RotDOF[a]	Number of rotational degrees of freedom, n_{rot}	Diatomic molecule	2
Rbond[a]	Length of molecular bond, R	Fit, this work	1.5×10^{-8} cm
VibDOF[a]	Number of vibrational degrees of freedom, nvib	Diatomic molecule	1
Theta_vib[a]	Vibrational Debye temperature	Fit, this work	2000 K
LJ_flag[a]	Flag for Mie potential, or Morse potential	Fit, this work	1
a_exp[a]	Power in Mie potential, a	Fit, this work	1.7
Z(1)	Atomic number of element 1	O	8
COT(1)	Atomic fraction of element 1	O makes up 2/3 of atoms in SiO_2	0.66667
Z(2)	Atomic number of element 2	Si	14
COT(2)	Atomic fraction of element 2	Si makes up 1/3 of atoms in SiO_2	0.33333

[a]New entries created by current modifications to ANEOS.

Lauson 1972b). Although this is a generally good description of the interaction of atoms held together by metallic bonds, it is not a good approximation for molecular binding forces, which are better described by a Lennard-Jones type of potential (Kittel 1971). Moreover, experience with the Morse potential for geologic materials has shown that it often results in a critical point that is obviously in the wrong place, and cannot be corrected by the facilities provided in ANEOS. Figure 7 below illustrates the pathologic shape of the phase curve on a *P*-*S* plot when the Morse potential is used for SiO_2. This is pathologic because of its broad top and close approach to a double peak. If an actual double peak were to develop, no unique critical point could be defined.

Russian studies of the interatomic potential (Bobrovskii et al. 1974; Zharkov and Kalinin 1971) suggest that for $\eta < 1$, the cold pressure can be written in a form first proposed by Mie (1903):

$$P_{\text{cold}} = C(\eta^m - \eta^a) \qquad 0 \le \eta < 1 \tag{4}$$

where $m > a$ to ensure that P_{cold} is always tensional. Note that $P_{\text{cold}} = 0$ in the limits of $\eta = 0$ and 1, as it must. Although Equation 4 closely resembles the Mie potential (of which the widely used Lennard-Jones potential is a particular case), it is really somewhat different because it is limited to densities lower than the reference (equilibrium) density. The exponents in this fit may thus differ from the exponents that fit molecular binding potentials most accurately because they are skewed to fit the pressure beyond the equilibrium separation. Nevertheless, in this paper I will refer to potentials of this type as "Mie potentials."

The constants C and m in Equation 4 are determined by the energy integral, Equation 3, and the continuity of $dP_{\text{cold}}/d\eta$ at $\eta = 1$, where it must match the slope of the cold-pressure curve for compressed states to yield the observed low-pressure bulk modulus. Thus, a is the only adjustable constant. The value of a reflects the long-range behavior of the interatomic potential (Zharkov and Kalinin 1971). For a solid bound mainly by Coulomb forces, $a = 4/3$, whereas for a molecular solid bound by Van der Waals forces, $a = 7/3$. A Lennard-Jones 6-12 potential also predicts $a = 7/3$. Here I choose a nominal value for a of 5/3 or about 1.7 after a similar choice by Bobrovskii et al. (1974), but any value can be chosen between about 1.2 and 3.0. The effect of varying a is to shift the position of the minimum of P_{cold} and thus of the critical point. The choice of a also affects the slope of the liquid/vapor phase curve because the vaporization energy (3) is a function of the exponent.

The problem of adjusting the critical point has been with ANEOS since its inception. Thompson and Lauson (1972b) included a term that can be added to the cold pressure in expanded states to move the critical point. This term was constructed so that it does not alter the separation energy, and so does not greatly affect the thermodynamic properties of the material far from the critical point. It thus cannot change the slope of the liquid-vapor phase curve. However, it does alter the shape of the free-energy curve and thus can change the critical ratio, a feature that was used in this study (Table 3 defines the adjustment parameters as inputs C53 and C54).

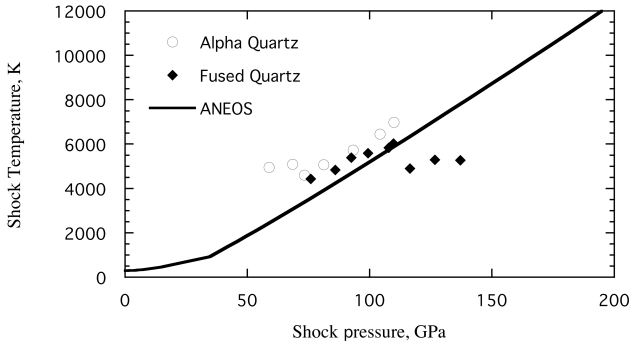

Fig. 10. Comparison of the measured shock temperatures of quartz and fused silica from Lyzenga (1983) to the ANEOS computation. Although the data show a wide scatter, perhaps due to the onset of melting on the Hugoniot at about 100 GPa (see text discussion), ANEOS seems to do a good job of approximating the observations.

Figure 6 shows the cold-pressure curves for SiO_2 with various choices of the constant a as well as the curve for the original Morse potential. Although all of these curves look very similar (as they must, because of the constraints on P_{cold} at both $\eta = 0$ and $\eta = 1$), there are clear differences in the positions of the minima. These differences are strongly reflected in the position of the critical point, so that adjustment of a is of great importance for constructing a successful EOS.

A somewhat technical point is that the density ρ_0 of the normal 1-bar, 273 K reference state of a material is slightly less than the cold reference density ρ_{00}, so that the reference state is actually in the expanded $\eta < 1$ region of the cold pressure. The internal interpolation used by ANEOS to derive cold-pressure parameters from the inputs reference density and bulk modulus must thus be substantially altered when the Mie potential is used.

THE "THERMAL" TERM IN THE HELMHOLTZ FREE ENERGY: MOLECULAR CLUSTERS

The "thermal" contribution to the Helmholtz free energy represents the temperature-dependent portion of the free energy in a material that ranges from a dense solid at low temperatures and high pressures to a dissociated gas at high temperatures and low densities. Although an equation good for any material over this broad range does not exist, an approximation adequate for hydrocode computations can be constructed by combining the free energy of a generalized Deybe solid with the monatomic gas limit. ANEOS thus employs the approximation:

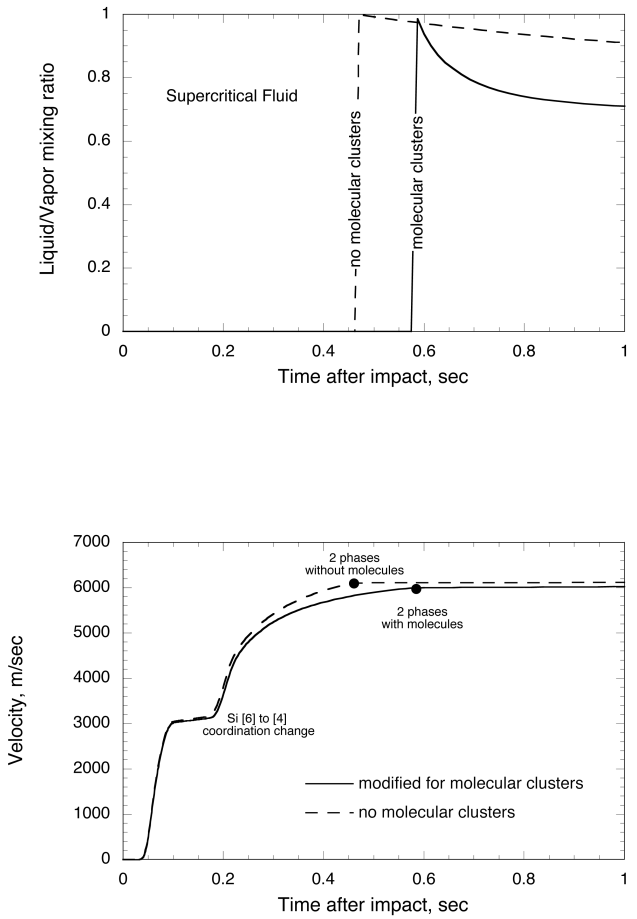

Fig. 11. Expansion velocity and liquid fraction as a function of time for a sphere of SiO_2 initially 5 km in radius starting from rest, at a point initially 4.3 km from the center. The initial conditions are density 5706 kg/m^3, internal energy 24.58 MJ/kg, entropy 4730 J/kg-K, temperature 15,800 K, and pressure 242 GPa. This is the shock state reached at a particle velocity of 7 km/s (the release curve is labeled 7 on Fig. 2: the entropy is shown in Fig. 7), simulating the vapor expansion from a Chicxulub-scale impact at an impact velocity of about 15 km/s. After 1 s, the velocity is essentially a linear function of radius (the maximum velocity is 8.6 km/s at the edge of the sphere, which is not shown here). The solid and dashed curves indicate the expansion conditions for the SiO_2 EOS with molecular clusters and without (as described in the caption for Fig. 7). Although the liquid/vapor ratio is substantially different when molecular clusters are present, the vapor expansion velocities are nearly identical, as are the pressure and temperature plots (not shown).

$$F_{\text{thermal}} = N_0 kT\left[3\ln(1-e^{-\theta/T}) - D(\theta/T) + \frac{3}{2}\frac{\ln(1+\psi^b)}{b}\right] \quad (5)$$

where θ is the Debye temperature (taken to be a function of density but not temperature in ANEOS), N_0 is the total number of atoms per unit mass, k is Boltzmann's constant, and D is the Debye integral, defined as:

$$D(x) = \frac{3}{x^3}\int_0^x \frac{y^3 dy}{e^y - 1} \quad (6)$$

The dimensionless function ψ(ρ, T) plays the role of an interpolation parameter that connects the solid and vapor states. This function was first defined in the Russian equation of state literature (Kormer et al. 1962), where it was used for a slightly different purpose, as a measure of the gas-like character of a substance. It is defined as:

$$\psi(\rho, T) = \frac{C_{13}\rho^{2/3}T}{\theta^2(\rho)} \quad (7)$$

where C_{13} is a dimensional constant that is chosen so that Equation 5 extrapolates to the free energy of a monatomic gas at high temperature. The constant b in Equation 5 is a convergence parameter ($0 < b \le 1$) recently introduced by Thompson (Thompson 1990) to improve the liquid/vapor phase convergence. It controls the rate at which ψ induces a transition between the solid and vapor limits. A value $b = 0.5$ is essential for the convergence of the SiO_2 EOS. If b is too large, Equation 5 may induce a second minimum in the Gibbs free-energy surface, leading to the unphysical occurrence of two critical points.

The function ψ is much less than 1 at low temperatures, and in this limit, Equation 5 extrapolates to a Debye solid. It vanishes at $T = 0$, and at temperatures well above the Debye temperature the first two terms approach [3ln(θ/T) − 1]. At high temperatures or low densities, ψ is much larger than 1, and in this limit the logarithm of ψ cancels the high-temperature Debye terms and, with a suitable choice of C_{13}, Equation 5 becomes equal to the Helmholtz free energy of a mixture of perfect, monatomic gases:

$$F_{thermal} \xrightarrow[T\to\infty]{} -kTN_0\sum_l \frac{N_l}{N_0}\left\{\ln\left[\frac{(2\pi m_l kT)^{3/2}}{N_l \rho h^3}\right]+1\right\} \quad (8)$$

where N_l is the number of atoms per unit mass of type l, m_l is the mass of each atom, and h is Planck's constant.

The challenge in generalizing this set of equations to contain molecular clusters is to leave the Debye terms unaffected while changing the way in which the gas phase is described. This amounts to finding a modification of ψ that preserves the low-temperature behavior, while extrapolating to a molecular gas at intermediate temperatures. Of course, at sufficiently high temperatures, the result should finally extrapolate to Equation 8. Although numerical methods exist for computing the precise chemical composition of a gas at any given temperature and pressure (Smith and Missen 1982), such a procedure is both too slow for efficient hydrocode computation and it requires a great deal of specialized

information, such as the heat capacities and formation energies of all chemical species over the full range of pressures and temperatures. In this paper I thus seek a middle way, adopting the philosophy of ANEOS itself, and attempt to find an analytic form that gives a good approximation to the final result without becoming too detailed. Once the desired analytic form is achieved, parameters in the equations are adjusted to fit the observed properties of the substance—in this case, SiO_2.

To achieve this result, suppose that the N_0 atoms in the material can undergo a reaction of the form:

$$mA + nB \rightleftharpoons A_mB_n \tag{9}$$

where there are only two types of atom, A and B, which can react to produce a molecule of composition A_mB_n. Although I will shortly confine attention to a diatomic reaction $m = n = 1$, the first step is kept more general. The Helmoltz free energy of this chemical system is written in terms of the partition functions ζ of each species (Denbigh 1971):

$$F_{\text{mol}} = -kT\ln(\zeta_A\zeta_B\zeta_C) \tag{10}$$

where ζ_A and ζ_B are the partition functions of a monatomic gas of A and B atoms:

$$\zeta_{A,B} = \frac{f_{A,B}^{N_{A,B}}}{N_{A,B}!}, \qquad \text{where} \tag{11}$$

$$f_{A,B} = \frac{1}{\rho}\left(\frac{2\pi m_{A,B}kT}{h^2}\right)^{3/2}$$

ζ_C is the partition function of the A_mB_n molecule. As before, $\zeta_C = f_C^{N_C}/N_C!$, where:

$$f_C = \frac{1}{\rho}\left(\frac{2\pi m_C kT}{h^2}\right)^{3/2} f_{\text{rot}} f_{\text{vib}} e^{E_B/kT} \tag{12}$$

In this equation, E_B is the binding energy of the molecular cluster and f_{rot} and f_{vib} are the polyatomic rotation and vibration partition functions:

$$f_{\text{rot}} = \left(\frac{\mu R^2 kT}{\hbar^2}\right)^{n_{\text{rot}}/2} \tag{13}$$

$$f_{\text{vib}} = \left(\frac{1 - e^{-E_B/kT}}{1 - e^{-\theta_{\text{vib}}/T}}\right)^{n_{\text{vib}}}$$

where μ is the reduced mass of the molecular cluster, R the radius of the cluster, n_{rot} is the number of rotational degrees of freedom, n_{vib} is the number of vibrational degrees of freedom, and θ_{vib} is the "vibrational Debye temperature" (Fowler and Guggenheim 1949, pp. 96 and 98). These extra partition functions prove to be essential in achieving the correct entropy of the molecular gas. They both depend on temperature (but not density) in different ways, so they can be used to match a range of temperature dependences of the entropy.

The equilibrium number of molecules N_C at a given temperature and pressure is determined by minimizing the free energy, Equation 10, with respect to N_C, subject to the constraint that the total number of atoms of type A, $N_1 = N_A + mN_C$, and those of type B, $N_2 = N_B + nN_C$, are fixed. This minimization leads to an implicit equation for N_C:

$$\frac{(N_1 - mN_C)^m (N_2 - nN_C)^n}{N_C} = \frac{f_A^m f_B^n}{f_C} \tag{14}$$

Some algebraic manipulation using this equation and an expansion of Equation 10 will return the Helmholtz free energy of the gas to the form of Equation 8, plus an additional term:

$$F_{\text{mol}} = F_{\text{monatomic}} - kT\left[N_1\ln\left(\frac{N_1}{N_1 - mN_C}\right) + N_2\ln\left(\frac{N_2}{N_2 - nN_C}\right) - (m + n - 1)N_C\right] \tag{15}$$

Note that if $N_C = 0$ (no molecular clusters), then the additional term vanishes, as expected.

Equation 15 is solved for F_{mol} by first solving Equation 14 for N_C and then substituting. Because the various partition functions f depend on both temperature and density, the final result is also a function of temperature and density.

If desired, this complex equation could be used to compute the free energy of a gas with molecular clusters. However, for the purposes of rapid hydrocode evaluation, a number of simplifications can be made. In the first place, we assume that the material we are dealing with is a stoichiometric mixture of atoms, so that the condensed phase is composed of a mixture of A and B atoms that can be entirely consumed in the formation of A_mB_n clusters, with nothing left over. This is, in fact, a valid assumption for SiO_2, if quartz (or any of its polymorphs) is the starting material. In this case a simple relation exists between the numbers of atoms such that $N_1/N_2 = m/n$. Applying this relationship, Equation 15 reduces to a much simpler form:

$$F_{\text{mol}} = F_{\text{monatomic}} + kTN_0\left[\ln w + \left(\frac{m + n - 1}{m + n}\right)(1 - w)\right] \tag{16}$$

where the new function w is defined as the fraction of unbound atoms:

$$w \equiv 1 - \frac{(m + n)N_C}{N_0} \tag{17}$$

If none of the atoms are bound in clusters, then $w = 1$ and the extra term vanishes, as expected. The apparent divergence of the logarithm as w approaches 0 (all atoms bound in clusters) is cancelled by the temperature T that multiplies ln w: w approaches 0 only as T goes to zero, and one can show that the product actually vanishes in this limit.

A subtle but important point here is that although the correction to $F_{\rm mol}$ vanishes in the zero temperature limit, its derivative does not. Even worse, it diverges like $1/T$. The result of this divergence is that the energy, $E = F + TS$, acquires a constant term equal to $-E_B N_0/(m + n)$. This really makes good sense: it represents the shift in the reference state energy due to the binding energy of the molecular clusters. However, the energy E_{00} at zero temperature and pressure is now negative—a somewhat undesirable choice. This is corrected by adding a constant term equal to $E_B N_0/(m + n)$ back into $F_{\rm mol}$ that cancels this addition and keeps E_{00} at zero.

A more drastic simplifying assumption is that the resulting clusters are diatomic molecules. Thus, $m = n = 1$. In this case, Equation 14 for N_C reduces to a simple quadratic equation that can be rapidly solved. Otherwise, the equation for N_C is of order $m + n$ and, in general, requires numerical methods for solution. The idea that SiO_2 gas might be approximately diatomic is supported by the chemical equilibrium computations illustrated in Fig. 4, which indicate that the gaseous species SiO and O_2 predominate just above the vaporization temperature. Equation 16 does not exactly represent this case because it assumes that there is only one type of molecular cluster with one single binding energy. To represent the dissociation of SiO_2 correctly, at least two rather different binding energies, one each for the Si-O bond (energy 432 kJ/mole or 4.48 eV) and O-O bond (143 kJ/mole, or 1.48 eV) are needed (data reported here is from Pauling 1988), and the entropy of mixing of the two different species should be added. However, the mixing entropy is small compared to the entropy from the specific heat, and the bond energies are similar, so the error made in using a diatomic Helmholtz free energy for SiO_2 is not serious for the purposes of hydrocode computations.

The general equation for w is easily obtained in a form that is relatively easy to solve:

$$\frac{w^{m+n}}{1-w} = \frac{1}{m^m n^n}\left(\frac{m+n}{N_0}\right)^{m+n-1}\frac{f_A^m f_A^m}{f_C} \equiv y_{mn} \qquad (18)$$

where $y_{mn}(P, T)$ is a function that will play an important role in Equation 19 below and the equations introduced in the Appendix.

In the special case that the molecules are diatomic clusters of the (distinguishable) atomic species A and B, the fraction of unbound pairs is:

$$w = \sqrt{y_{11}}\left(\sqrt{y_{11}+2} - \sqrt{y_{11}}\right), \qquad \text{where} \qquad (19)$$

$$y_{11} = \frac{1}{N_0}\frac{f_A f_B}{f_C}$$

This form of the equation for w avoids numerical singularities and indicates the proper limits as y_{11} becomes either very large or very small.

Having solved for the molecular correction to the Helmholtz free energy, it remains to show how Equation 5, which is used by ANEOS, is corrected to incorporate these improvements. It is easy to show that a simple modification to ψ will accomplish this goal. Thus, the original function ψ in Equation 7 is multiplied by a function Z given by:

$$Z(\rho, T) = w^{2/3} e^{(1-w)/3} e^{E_B/(3kT)} \qquad (20)$$

The functions of w in this expression generate the additional terms in Equation 16 at high temperature (for $m = n = 1$; the generalization to other m and n is straightforward and is given explicitly in the Appendix), and the exponential term that includes E_B adds a constant to $F_{\rm mol}$ that corrects the zero point of E_{00}. This is the only fundamental change needed to ANEOS.

With this modification, the ANEOS equation of state now incorporates molecular clusters. Because Z is a function of both density and temperature, many expressions for quantities such as pressure, entropy, and energy acquire additional terms that must be incorporated in ANEOS. For reference, these additional terms are written out in the Appendix.

APPLICATION OF THE IMPROVED ANEOS TO SiO_2

Thompson's 1990 version of ANEOS (Thompson 1990) required the input of 37 parameters (in the more sophisticated "long" form. The older "short" form required 24.). Most of these are simple and can be readily determined from experimental or standard thermodynamic data. Some of the parameters control seldom-needed options, such as thermal conductivity or special convergence procedures. The modifications to the ANEOS equation of state described above add another 8 parameters, of which only 3 need serious work to determine, although even these parameters can be approximately determined from tables of thermodynamic or spectroscopic data. Unfortunately, these different parameters interact with one another in complex ways and it is not a straightforward process to derive a set of input parameters that adequately describes a given material.

The principal parameters affecting the liquid/vapor transition are the vaporization energy, $E_{\rm vap}$, and Debye temperature, θ_D, among the original 37 input variables. The vaporization energy has a major (but not unique) effect on the vaporization temperature, while the Debye temperature most

strongly affects the entropy of the condensed (liquid or solid) phase. Two new variables, the molecular binding energy, E_B and the vibrational Debye temperature, θ_{vib}, have strong effects on both the vaporization temperature and slope of the liquid/vapor phase boundary. E_B is the energy (in eV) necessary to break the average molecular bond and θ_{vib} is the average spacing between vibrational energy levels $\overline{\Delta E}$ divided by Boltzmann's constant k: $\theta_{vib} = \overline{\Delta E}/k$. Other new parameters, such as the number of vibrational and rotational degrees of freedom, are set by the structure of the molecules in the vapor (they are equal to 2 and 1, respectively, for diatomic molecules). The parameter a describing the Mie potential has little effect on most thermodynamic quantities, but plays an important role in adjusting the position of the critical point along the liquid/vapor phase curve, and the critical entropy. The radius of the molecules in the gas, R, has only a minor effect on other quantities, and was set equal to a generic value of 1.5×10^{-10} m. In the actual process of seeking a good fit between the observed properties of SiO_2 and its measured thermodynamic properties, four basic properties, listed in Table 2, were used to target a search for the four parameters described above. Because all of these parameters interact, my actual procedure, after using thermodynamic tables to establish approximate values, was to numerically construct a matrix of derivatives of each of the four target quantities with respect to the four input parameters, and to manually seek a best solution, also listed in Table 2. This process could probably be automated to yield a better fit in some more objective sense, such as least squares deviation, but in view of other misfits (see below) and uncertainties in the target parameters listed in Table 2, this enhanced precision may be misleading. In any event, the parameter set in Table 3 yields good agreement between the target and computed quantities.

Of the parameters in Table 2, the vaporization temperature T_{vap} and the pressure at the triple point, P_Δ (I take this as nearly equal to the pressure of the empirical liquid/vapor phase curve extrapolated to the melting point of high cristobalite, 1996 K), together determine the slope of the phase curve on the Arrhenius plot, which is also related to the difference between the liquid and vapor entropies. The vapor entropy plays an important role in the mass fraction of vapor produced. This property is most strongly affected by the presence of molecular clusters.

One input parameter whose derivation may not be obvious is the value of Gruneisen's gamma in the alpha quartz reference state, Γ_0. This parameter measures the dependence of pressure on internal energy (Poirier 1991), and equals the following combination of physical constants:

$$\Gamma_0 = \frac{aK_0}{\rho_0 C_V} \tag{21}$$

where α is the volume coefficient of thermal expansion, 3.4×10^{-5} K^{-1} (Skinner 1966), K_0 is the bulk modulus, 3.759×10^{10} Pa (Birch 1966), ρ_0 is the reference density, 2650 kg/m^3, and C_V is 781 J/kg-K (Weast 1972). Taking these values together yields $\Gamma_0 = 0.618$ for alpha quartz, as entered in Table 3.

Table 3 summarizes a set of input parameters that gives a good description of the substance SiO_2 at high pressure and temperature. The large density change in the quartz-stishovite transition shows up clearly in the Hugoniot curve, Fig. 5, so it is important to include this high-pressure phase transition. As discussed above, this precludes a detailed treatment of a separate liquid phase in the present version of ANEOS, so that liquid and solid phase are treated as a single condensed phase. This is probably not as serious as it may seem, because the density contrast between liquid and solid phases is only of order 10%, while that between quartz and stishovite approaches a factor of 1.5.

Figure 5 shows that the choice of parameters in Table 3 yields a good match between the measured shock data (Trunin et al. 1971) and the observed Hugoniot curve up to the exceptionally high particle velocity of 12.3 km/s, or to a corresponding pressure of 652 GPa. These highly compressed states are insensitive to the presence of molecular clusters and modifications of the expanded state, but do depend strongly on the presence of a high-pressure phase transition. The ANEOS modifications described in this paper are seen most acutely in the liquid/vapor phase curve. Figure 8 shows that the choice of parameters in Table 2 gives an excellent fit to a variety of data on the phase curve in P and T. Figure 7 indicates that these parameters also give a good representation of the liquid/vapor transition in the important P versus S variables. Figure 9 shows that, at 1 bar, the dependence of entropy on temperature computed by ANEOS agrees with that computed from the HSC chemistry package in overall value up to about 5000 K, but does not show the same detailed temperature dependence. This is a consequence of my approximation of two binding energies as one. Thus, the first sharp rise in entropy above the vaporization temperature is due to O_2 dissociation, whereas the second is due to SiO dissociation (compare Fig. 4b). ANEOS averages over these two steps with a single, monotonic rise of entropy. A more complicated addition to ANEOS could correct this, but at the present state of hydrocode computations, such fine details do not seem to warrant the extra complication and computation time.

Figure 10 plots the predicted shock temperatures against the limited data that exists on this quantity. The ANEOS prediction steers a middle course between the data for either fused quartz or crystalline alpha quartz between 50 and 150 GPa. This is probably because the high-pressure melting curve for quartz (Ivanov 2003) intersects the Hugoniot at about 100 GPa, just where the shock temperature seems to drop off as pressure increases above 100 GPa in Fig. 10. Because this ANEOS parameterization of the SiO_2 equation of state does not include a solid-melt transition, it cannot properly model the temperature change in this pressure range.

What ANEOS cannot do is account for metastable states. It assumes perfect thermodynamic equilibrium and thus perfect reversibility of phase transitions. It thus cannot account for the formation of post-shock metastable stishovite or coesite, although these are observed in shock release experiments (Ahrens and Rosenberg 1968). It is also unable to account for a kinetic delay in the onset of high-pressure phase transformations, and so may predict shock-wave splitting (Zel'dovich and Raizer 1967) in the ranges of shock compression just before the nominal formation pressure of stishovite, although such splitting is not observed in practice (Trunin et al. 1971). This may account for the mismatch between the ANEOS Hugoniot and the data of Turnin (1971) below a particle velocity of 1 km/s, although some of the discrepancy is likely due to the difference between single crystal and polycrystalline quartz targets.

APPLICATION TO AN EXPANDING CLOUD OF HOT SILICA

Having gone to a great deal of trouble to correct the ANEOS equation of state to better represent SiO_2, it is important to see how this correction affects the outcome of numerical hydrocode computations. For this purpose, I constructed a very simple model of an expanding spherical cloud of hot silica. The model was begun with a sphere 10 km in diameter of SiO_2 at rest, with a uniform initial pressure of 242 GPa and a temperature of 15,800 K. These conditions were chosen to represent the outcome of an impact that generates a particle velocity of 7 km/s in quartz, which is approximately the same as the conditions of the K/Pg Chicxulub crater impact. The entropy of this initial state is 4730 J/kg-K, which is approximately the critical point entropy (see the arrow in Fig. 7).

The expansion of this ball of hot gas was computed using a simple Lagrangian hydrocode that divided the sphere into 30 concentric shells, where the radius of each successive shell was chosen to contain equal amounts of mass. The pressure of this sphere was dropped to zero at $t = 0$, when the mass begins to expand freely into the space around it. The time evolution of temperature, pressure, velocity, and position (along with all other thermodynamic variables computed by ANEOS) was recorded at each time step, and the results are plotted in Fig. 11. A second computation was performed with the same initial conditions and EOS, with the one difference that molecular clusters were not present in the second EOS, as described in the caption of Fig. 7. As expected, the entropy remains constant during the expansion, although the temperature and pressure both fall rapidly.

Figure 11a shows that the SiO_2 remains in a supercritical state for about the first half-second of the expansion (see also the curve labeled "7" in Fig. 2, which illustrates the full thermodynamic path). Liquid first appears at about 0.47 s when no molecular clusters are present, but is delayed until about 0.58 s when molecules can form. However, because of the high cost of vapor formation in the absence of molecular clusters, by 1 s the EOS without molecules produced only about 10 wt% of vapor, whereas that with molecules generated about 30 wt% of vapor, an increase of a factor of 3. This difference persists through the end of the computation at 1000 s (not shown in the figure because little change occurs after 1 s). Thus, as expected, the molecular cluster modification results in a substantial increase in the amount of vapor produced in an impact of this kind.

Figure 11b illustrates the velocity of the test point as a function of time after the beginning of expansion. The test point, located 0.7 km from the edge of the sphere, remains nearly at rest until the rarefaction wave arrives 0.05 s after the pressure is released at the sphere's surface. It then accelerates rapidly to about 3 km/s. At about 0.1 s it coasts at nearly constant velocity for another 0.07 s before it again begins to accelerate.

This coasting is due to the high-to-low pressure transformation from stishovite to quartz, a modification in ANEOS to the cold-pressure term, which is added to the EOS for any temperature in Equation 2. Although this might at first seem like a flaw in the formulation of the EOS at high temperatures, there is evidence from Raman spectral studies of anorthite glass (Daniel et al. 1997) and of silica (Hemley et al. 1994) that such a density changes actually does occur in the liquid due to the change of Si coordination from six-fold to four-fold, thus echoing the stishovite-quartz transformation built into ANEOS. What may not be correct is the lack of temperature dependence of this transition in ANEOS, so that the pressure and temperature at which this coasting takes place (about 50 GPa and 13,000 K) may be too high (observationally, it is about 25 GPa at room temperature (Hemley et al. 1994), and so would occur later in the expansion, but still before the critical point is reached).

About 0.4 s after expansion starts, the test particle has reached a nearly constant expansion velocity of about 6 km/s. At this time, the velocity in the expanding sphere is a nearly linear function of distance from its center, and the remainder of its evolution is a constant-velocity coast to larger radii, with a density profile very similar to that expected from analytic models of gas-cloud expansion (Zel'dovich and Raizer 1967). Because energy is conserved in the expansion process, this final velocity is nearly the same for both versions of the EOS. The only difference is that the sphere without molecules expands slightly faster, as shown in Fig. 11b, because the lack of molecular clustering gives it a higher pressure and thus drives a slightly more vigorous expansion. The figure also shows the time at which the two-phase saturation vapor curve is reached on both expansion histories. Note that little acceleration occurs once both liquid and vapor phases are present below the critical point. This is a consequence of the high compressibility of a two-phase gas/liquid mixture at equilibrium (the compressibility is not actually infinite because the temperature is also changing during this adiabatic expansion).

Thus, the introduction of molecular clusters has little overall effect on the expansion velocity of a shocked mass of silica, but it does have a strong effect on the amount of liquid and vapor produced in such an event. Vapor fractions are increased dramatically by the formation of molecular clusters in the vapor phase.

CONCLUSIONS

The modified ANEOS equation of state provides a good general representation of a complex material with a liquid/vapor phase transition, molecular clusters in the vapor state, and an important high-pressure phase transformation. It cannot yet represent a distinct liquid/solid transition, and the high-pressure phase transformation does not depend correctly on temperature. However, it does represent a step forward in the realistic representation of the EOS of a complex geologic material at pressures and temperatures that are important in the early phases of impact processes. This improvement is needed for the proper treatment of melting and vaporization in impacts, especially the accurate computation of the mass and physical state of fast early ejecta from impact craters. Because of the recent recognition of widespread distal deposits of Archean impacts (Simonson and Glass 2004), the ability to accurately compute this ejecta component has become important for interpreting this phase of Earth history. Similarly, the distribution of the distal ejecta of the Chicxulub impact (Alvarez et al. 1995; Kring and Durda 2002; Melosh et al. 1990) has become an important issue for understanding the nature of this great biological extinction.

The molecular modifications described in this paper apply only to a material with diatomic molecules in the vapor phase. Fortunately, this approximation applies not only to SiO_2, but also to a variety of other interesting geologic materials (Ahrens and O'Keefe 1972). It can thus be expected that successful ANEOS equations of state may be constructed for many common geologic materials. The one interesting material that the diatomic modification of ANEOS cannot accommodate is water. In spite of several attempts to force-fit the diatomic model to the properties of water, it proved impossible to properly represent the entropy of the vapor phase with such a model. For water, the temperature range between the evaporation of triatomic molecules from the liquid and their dissociation into individual atoms is very broad (from 273 K to about 4000 K at 1 bar), so triatomic molecules dominate the vapor phase over a large portion of the phase diagram. For this reason, the diatomic analysis was extended to triatomic and larger molecular clusters, as described in the Appendix.

Accurate EOSs for geologic materials like SiO_2 at very high pressures and temperatures are essential for further progress in the study of planetary impact cratering. My hope is that this paper represents only the first step in improving our knowledge of the behavior of earth materials at extreme conditions.

Acknowledgments–Boris Ivanov has made many contributions to my study of EOSs since at least 1990, and his knowledge of Russian efforts in this area has greatly widened my understanding of some subtle problems. His question about vibrational degrees of freedom in the gas phase lead to great improvements in my computation of the entropy of vaporized SiO_2. He and Seiji Sugita also provided helpful reviews. Betty Pierazzo contributed greatly to methods of determining EOS parameters, and constructed ANEOS parameter sets for water, basalt and granite. Abby Sheffer showed me how to use the HSC program and compute entropy from its output. Early work on this EOS was supported by NASA's PGG program under grant NAG5-11493. The most recent work on $SiO_2$was funded by NASA Cosmochemistry grant NAG5-12854. I also thank the German Humboldt Foundation for providing financial support in 2005 and 2006 and the Bavarian Geological Institute for hospitality while this paper was in preparation.

This paper is dedicated to Prof. Dieter Stöffler on the occasion of his retirement from active supervision of the Humboldt Museum in Germany. Prof. Stöffler has enjoyed a long career devoted to the study of meteorite impacts and the mineralogical changes caused by the high pressures that develop in impacts. Judging by his papers, one of his favorite minerals is quartz, or more generally, SiO_2. He recently published two definitive studies of the high-pressure modifications of quartz (Grieve et al. 1996; Stöffler and Langenhorst 1994).

Editorial Handling—Dr. Elisabetta Pierazzo

REFERENCES

Ahrens T. J. and O'Keefe J. D. 1972. Shock melting and vaporization of lunar rocks and minerals. *The Moon* 4:214–249.

Ahrens T. J. and Rosenberg J. T. 1968. Shock metamorphism: Experiments on quartz and plagioclase. In *Shock metamorphism in natural materials*, edited by French B. M. and Short N. M. Baltimore, Maryland: Mono Book Corp. pp. 59–81.

Alvarez W., Claeys Ph., and Kieffer S. W. 1995. Emplacement of Cretaceous-Tertiary boundary shocked quartz from Chicxulub crater. *Science* 269:930–935.

Anderson C. E. 1987. An overview of the theory of hydrocodes. *International Journal of Impact Engineering* 5:33–59.

Anderson O. L. 1995. *Equations of state of solids for geophysics and ceramic science*. New York: Oxford University Press. 430 p.

Barin I. 1989. *Thermochemical data of pure substances*. Weinheim, Germany: VCH Verlags Geselleschaft. 1739 p.

Birch F. 1966. Compressibility: Elastic constants. In *Handbook of physical constants*, edited by Clark S. P. New York: Geological Society of America. pp. 107–173.

Bobrovskii S. V., Gogolev V. M., Zamyshlyaev B. V., and Lozhkina V. P. 1974. Spalling rate in a solid medium subjected to a strong shock wave. *Combustion, Explosion, and Shock Waves* 10:799–805.

Centolanzi F. J. and Chapman D. R. 1966. Vapor pressure of tektite glass and its bearing on tektite trajectories determined from

aerodynamic analysis. *Journal of Geophysical Research* 71: 1735.
Chase M. W. 1998. *NIST-JANAF thermochemical tables*. Woodbury, New York: American Chemical Society. 1951 p.
Daniel I., Gillet P., McMillan P. F., Wolf G., and Verhelst M. A. 1997. High-pressure behavior of anorthite: Compression and amorphization. *Journal of Geophysical Research* 102:10,313–10,325.
Denbigh 1971. *The principles of chemical equilibrium*. Cambridge: Cambridge University Press. 494 p.
Fowler R. H. and Guggenheim E. A. 1949. *Statistical thermodynamics*. Cambridge: Cambridge University Press. 701 p.
Grieve R. A. F., Langenhorst F., and Stöffler D. 1996. Shock metamorphism of quartz in nature and experiment: II. Significance in geoscience. *Meteoritics & Planetary Science* 31: 6–35.
Hemley R. J., Prewitt C. T., and Kingma K. J. 1994. High-pressure behavior of silica. In *Silica, physical behavior, geochemistry, and materials applications*, edited by Heaney P. J., Prewitt C. T., and Gibbs G. V. Washington, D.C.: Mineralogical Society of America. pp. 41–81.
Hidalgo H. 1960. Ablation of glassy material around blunt bodies of revolution. *ARS Journal* 30:806–814.
Hirschfelder J. O., Curtiss C. F., and Bird R. B. 1964. *Molecular theory of gases and liquids*. New York: Wiley and Sons. 1219 p.
Ivanov B. A. 2003. Modification of ANEOS for rocks in compression. In *Impact cratering: Bridging the gap between modeling and observation*. Houston, Texas: Lunar and Planetary Institute. 40 p.
Kieffer S. W. and Delany J. 1979. Isentropic decompression of fluids from crustal and mantle pressures. *Journal of Geophysical Research* 84:1611–1620.
Kittel C. 1971. *Introduction to solid state physics*. New York: Wiley. 766 p.
Kormer S. B., Funtikov A. I., Urlin V. D., and Kolesnikova A. N. 1962. Dynamic compression of porous metals and the equation of state with variable specific heat at high temperatures. *Soviet Physics JETP* 15:477–488.
Kring D. A. and Durda D. D. 2002. Trajectories and distribution of material ejected from the Chicxulub impact crater: Implications for postimpact wildfires. *Journal of Geophysical Research* 107: 1–22.
Lyzenga G. A., Ahrens T. J., and Mitchell A. C. 1983. Shock temperatures of SiO_2 and their geophysical implications. *Journal of Geophysical Research* 88:2431–2444.
Marsh S. P. 1980. *LASL shock Hugoniot data*. Berkeley: University of California Press. 658 p.
Melosh H. J. 1989. *Impact cratering: A geologic process*. New York: Oxford University Press. 245 p.
Melosh H. J. and Pierazzo E. 1997. Impact vapor plume expansion with realistic geometry and equation of state. 28th Lunar and Planetary Science Conference. pp. 935–936.
Melosh H. J., Schneider N. M., Zahnle K. J., and Latham D. 1990. Ignition of global wildfires at the Cretaceous/Tertiary boundary. *Nature* 343:251–254.
Mie G. 1903. Zur kinetischen Theorie der einatomigen Körper. *Annalen der Physik* 11:657–697.
Mysen B. O. and Kushiro I. 1988. Composition, evaporation, melting, and crystallization in the primitive solar nebula: Experimental data in the system MgO-SiO_2-H_2 to 1.0×10^{-9} bar and 1870 °C with variable oxygen fugacity. *American Mineralogist* 73:1–19.
Pauling L. 1988. *General chemistry*. New York: Dover. 959 p.
Poirier J.-P. 1991. *Introduction to the physics of the Earth's interior*. Cambridge: Cambridge University Press. 264 p.
Presnall D. C. 1995. Phase diagrams of earth-forming minerals. In *Mineral physics and crystallography: A handbook of physical constants*, edited by Ahrens T. J. Washington, D.C.: American Geophysical Union. pp. 248–268.
Roine A. 2002. Outokumpu HSC Chemistry for Windows, Version 5. Outokumpu Research Oy, Finland.
Schaefer L. and Fegley B. 2004. A thermodynamic model of high temperature lava vaporization on Io. *Icarus* 169:216–241.
Schick H. L. 1960. A thermodynamic analysis of the high-temperature vaporization properties of silica. *Chemical Reviews* 60:331–362.
Sengers J. L. 2002. *How fluids unmix*. Amsterdam: Royal Netherlands Academy of Arts and Sciences. 302 p.
Shornikov S. I., Archakov I. Y., and Shul'ts M. M. 1998a. Mass spectrometric study of vaporization and thermodynamic properties of silicon dioxide. I. Composition of the gas phase and partial vapor pressures of the molecular forms over silicon dioxide. *Russian Journal of General Chemistry* 68:1171–1177.
Shornikov S. I., Archakov I. Y., and Shul'ts M. M. 1998b. Mass spectrometric study of vaporization and thermodynamic properties of silicon dioxide. II. Determination of partial vaporization coefficients of silicon dioxide. *Russian Journal of General Chemistry* 69:187–196.
Shornikov S. I., Archakov I. Y., and Shul'ts M. M. 1998c. Mass spectrometric study of vaporization and thermodynamic properties of silicon dioxide. III. Equilibrium reactions of molecules occurring in the gas phase over silica. *Russian Journal of General Chemistry* 70:360–370.
Simonson B. M. and Glass B. P. 2004. Spherule layers—Records of ancient impacts. *Annual Review of Earth and Planetary Sciences* 32:329–362.
Skinner B. J. 1966. Thermal expansion. In *Handbook of physical constants*, edited by Clark S. P. New York: Geological Society of America. pp. 75–96.
Smith W. R. and Missen R. W. 1982. *Chemical reaction equilibrium analysis*. New York: Wiley. 364 p.
Stöffler D. and Langenhorst F. 1994. Shock metamorphism of quartz in nature and experiment: I. Basic observation and theory. *Meteoritics & Planetary Science* 29:155–181.
Thompson S. L. 1973. Improvements in the CHART D energy flow-hydrodynamic code V: 1972/1973 modifications. Albuquerque, New Mexico: Sandia National Laboratories. 196 p.
Thompson S. L. 1990. ANEOS: Analytic equations of state for shock physics codes input manual. Albuquerque, New Mexico: Sandia National Laboratories. 57 p.
Thompson S. L. and Lauson H. S. 1972a. Improvements in the CHART D energy flow-hydrodynamic code II: A revised program. Albuquerque, New Mexico: Sandia National Laboratories. 309 p.
Thompson S. L. and Lauson H. S. 1972b. Improvements in the Chart D radiation-hydrodynamic CODE III: Revised analytic equations of state. Albuquerque, New Mexico: Sandia National Laboratories. 119 p.
Tillotson J. H. 1962. Metallic equations of state for hypervelocity impact. San Diego: General Dynamics. 141 p.
Trunin R. F., Simakov G. V., Podurets M. A., Moiseyev B. N., and Popov L. V. 1971. Dynamic compressibility of quartzite at high pressure. *Izvestiya Akademii Nauk SSSR*, English translation 1: 13–20.
Wackerle J. 1962. Shock-wave compression of quartz. *Journal of Applied Physics* 3:922–937.
Walter L. S. and Carron M. K. 1964. Vapor pressure and vapor

fractionation of silicate melts of tektite composition. *Geochimica et Cosmochimica Acta* 28:937–951.
Weast R. C. 1972. Chemical Rubber Handbook. Cleveland, Ohio: CRC Press.
Young D. A. and Alder B. J. 1971. Critical point of metals from the van der Waals model. *Physical Review A* 3:364–371.
Zel'dovich Y. B. and Raizer Y. P. 1967. *The physics of shock waves and high temperature hydrodynamic phenomena*. New York: Academic Press. 916 p.
Zharkov V. N. and Kalinin V. A. 1971. *Equations of state for solids at high pressures and temperatures*. New York: Consultants Bureau. 257 p.

APPENDIX: ANEOS MODIFICATION FOR MOLECULAR CLUSTERS

The Thermal Terms in the Helmhotz Free Energy section describes the modifications needed to incorporate molecular clusters into the Helmholtz free energy. The basic modification is the replacement of the interpolation function ψ, in Equation 5, by the product $Z\psi$, where Z is defined in Equation 21. Although this completes the changes needed to revise the Helmholtz free energy, the expressions used by ANEOS for pressure, entropy, etc. are all modified and acquire additional terms through derivatives of Z. In this appendix I will not repeat the basic equations used by ANEOS, as these are reported in Thompson (1990) and Thompson and Lauson (1972b). They are correctly updated by the simple replacement of ψ by $Z\psi$.

The expression for Z in the special case of a binary compound was given in the text as Equation 21. The general expression for any values of m and n is:

$$Z(\rho, T) = \left[w e^{\left(1-\frac{1}{m+n}\right)(1-w)} e^{\frac{E_B}{(m+n)kT}} \right]^{2/3} \tag{A1}$$

Two new functions of Z will make these new expressions more compact. Define:

$$\alpha(\rho, T) = -\frac{3}{2}\frac{\rho}{Z}\frac{\partial Z}{\partial T}\bigg|_T \tag{A2}$$

$$\beta(\rho, T) = \frac{T}{Z}\frac{\partial Z}{\partial T}\bigg|_\rho$$

These functions are most readily expressed in terms of a new auxiliary function H_1:

$$\alpha = -\frac{3}{2}\frac{\partial \ln y_{mn}}{\partial \ln \rho} H_1 = \frac{3}{2}(m+n-1)H_1 \tag{A3}$$

$$\beta = \frac{\partial \ln y_{mn}}{\partial \ln T} H_1 - \frac{2}{3(m+n)}\frac{E_B}{kT}$$

where the function y_{mn} is defined in the text by Equation 18, and

$$H_1 = \frac{2(1-w)}{3(m+n)} \tag{A4}$$

Subsequent equations will also require derivatives of α and β with respect to density ρ and temperature T. These derivatives can be expressed in terms of H_1 and a second auxiliary function H_2:

$$\rho\frac{\partial \alpha}{\partial \rho} = -\frac{3}{2}H_1 H_2 \left(\frac{\partial \ln y_{mn}}{\partial \ln \rho}\right)^2 \tag{A5}$$

$$T\frac{\partial \alpha}{\partial T} = -\frac{3}{2}H_1 H_2 \left(\frac{\partial \ln y_{mn}}{\partial \ln T}\right)\left(\frac{\partial \ln y_{mn}}{\partial \ln \rho}\right)$$

$$T\frac{\partial \beta}{\partial T} = H_2 H_2 \left(\frac{\partial \ln y_{mn}}{\partial \ln T}\right)^2 + H_1\left(\frac{\partial^2 \ln y_{mn}}{\partial \ln T^2}\right) + \frac{2}{3(m+n)}\frac{E_B}{kT}$$

where

$$H_2 = \frac{\partial \ln H_1}{\partial \ln y_{mn}} = -\frac{w}{(m+n)-(m+n-1)w} \tag{A6}$$

In the following equations for pressure P, entropy S, energy E, heat capacity C_V, and the derivatives $\partial P/\partial \rho$ and $\partial P/\partial T$, it is understood that the symbol ψ stands for the product of Z and the original version of ψ in Equation 7. The modifications to the basic ANEOS quantities are thus:

$$P = P_{old} - \rho N_0 kT\left(\frac{\psi^b}{1+\psi^b}\right)\alpha \tag{A7}$$

$$S = S_{old} - \frac{3}{2}N_0 k\left(\frac{\psi^b}{1+\psi^b}\right)\beta \tag{A8}$$

$$E = E_{old} - \frac{3}{2}N_0 kT\left(\frac{\psi^b}{1+\psi^b}\right)\beta \tag{A9}$$

$$C_V = C_{Vold} \tag{A10}$$

$$-\frac{3}{2}N_0 k\left(\frac{\psi^b}{1+\psi^b}\right)\left[\beta\left(1+\frac{b(2+\beta)}{1+\psi^b}\right) + T\frac{\partial \beta}{\partial T}\right]$$

$$\frac{\partial P}{\partial \rho} = \frac{\partial P_{old}}{\partial \rho} - N_0 kT\left(\frac{\psi^b}{1+\psi^b}\right) \tag{A11}$$

$$\left\{\alpha + \left[1 + \frac{2b}{3}\,\frac{2(1-3\Gamma)-\alpha}{1+\psi^b}\right] + \rho\frac{\partial \alpha}{\partial \rho}\right\}$$

$$\frac{\partial P}{\partial T} = \frac{\partial P_{old}}{\partial T} - \rho N_0 k \left(\frac{\psi^b}{1+\psi^b} \right) \left\{ \alpha + \frac{b[\alpha(1+\beta) - \beta(1-3\Gamma)]}{1+\psi^b} + T\frac{\partial \alpha}{\partial T} \right\} \quad \text{(A12)}$$

where Γ is a function of the Debye temperature θ defined as (Thompson and Lauson 1972b):

$$\Gamma(\rho) = \frac{\rho}{\theta}\frac{d\theta}{d\rho} \quad \text{(A13)}$$